Dilute Nitride Semiconductors
Edited by M. Henini

Chapter 7

Measurement of Carrier Localization Degree, Electron Effective Mass, and Exciton Size in $In_xGa_{1-x}As_{1-y}N_y$ Alloys

A. Polimeni, F. Masia, G. Baldassarri Höger von Högersthal, M. Felici and M. Capizzi

INFM-Dipartimento di Fisica, Universita' di Roma "La Sapienza", Piazzale A. Moro 2, 00185 Roma, Italy

ABSTRACT

We employ photoluminescence under a magnetic field to investigate the electronic properties of $In_xGa_{1-x}As_{1-y}N_y$/GaAs heterostructures. We studied samples with nitrogen concentration from the doping ($y < 0.01\%$) to the alloy ($y = 5\%$) limit. In the alloy limit, we found that the origin of the radiative recombination at low temperatures (T lower than 100 K) is not excitonic, contrary to previous assignments, and is due to free holes recombining with electrons localized in N-rich regions. The evolution of the electron effective mass, m_e, and exciton radius, r_{exc}, was studied in $GaAs_{1-y}N_y$ epilayers and quantum wells with N concentration varying from $y < 0.01\%$ to $y = 2.0\%$. In particular, by exploiting the capability of post-growth hydrogen irradiation to fine tune the electronic properties of $GaAs_{1-y}N_y$, we are able to assess that a major change in m_e and in r_{exc} takes place within a very narrow interval of N concentrations, which is centred at $y = 0.1\%$. Alloying of $GaAs_{1-y}N_y$ with In ($x \sim 0.3$) results in a shift of such interval to $y = 1.0\%$.

7.1. INTRODUCTION

Recently, nitrogen incorporation in $In_xGa_{1-x}As$-based materials has attracted much interest owing to the strong modifications exerted by N on the band structure of the host lattice. These include a giant bandgap reduction [1–4] and a decrease in the rate at which the bandgap depends on hydrostatic pressure [5–8] and temperature [5,9–18]. Moreover, a strong dependence of the electron effective mass, m_e, on the nitrogen concentration has been found by a variety of experimental techniques [19–32]. The introduction of N in the host lattice is also a source of a high degree of disorder, which manifests itself on the optical properties of the material. This leads to a sizeable

inhomogeneous broadening of the radiative transitions [11], to a large Stokes shift between absorption and emission [33], and to the presence of localized states, which at low temperatures dominate often the emission spectra [11,12,17,34–37]. It has been shown that localization phenomena in $In_xGa_{1-x}As_{1-y}N_y$ reflects on the electron transport too [38,39]. Furthermore, $In_xGa_{1-x}As_{1-y}N_y$ alloys show surprising effects when irradiated with atomic hydrogen. Indeed, our group reported a fully tunable and reversible variation of the electronic (i.e. bandgap value, response to temperature changes, effective mass, and exciton radius) and structural (lattice constant and lattice vibrational properties) properties of $In_xGa_{1-x}As_{1-y}N_y$ by means of ex situ H irradiation [40–49]. In particular, H passivates N atoms in the lattice leading to an effective N concentration, which has allowed us to study the evolution of the material's properties with N concentration in a very careful manner. The microscopic origin of the surprising effects of H in $In_xGa_{1-x}As_{1-y}N_y$ has been investigated theoretically by many groups [50–57] and it has been established that the formation of a specific N-dihydrogen complex (referred to as $N–H_2^*$) is responsible for N passivation. This picture has been questioned very recently on the grounds of infrared absorption measurements [58].

Here, we report on a comprehensive study of the effects of a magnetic field ($B = 0–12$ T) on the photoluminescence (PL) properties of $In_xGa_{1-x}As_{1-y}N_y$/GaAs heterostructures. The samples investigated and the experimental methods employed are described in Section 7.2. In Section 7.3, we show that the shift of the PL peak energy induced by B decreases sizably and changes its dependence on B from linear to quadratic on going from low to high T. These findings indicate that the PL emission at low temperatures is not excitonic and it is determined, instead, by the recombination of loosely bound electron–hole pairs in which one carrier (electron) is localized by N-induced potential fluctuations and the other carrier (hole) is delocalized. Section 7.4 describes electron effective mass measurements. First, we review the data reported in the literature and the different methods used for obtaining those data. Then, we describe the evolution of the electron effective mass in $GaAs_{1-y}N_y$ epilayers when N concentration varies from the dilute limit ($y < 0.01\%$) to the alloy limit ($y = 0.5\%$) as measured by magneto-PL. By exploiting the capability of H to tune the bandgap of $GaAs_{1-y}N_y$, we asses that a major increase in m_e occurs for $y \sim 0.1\%$. This change in m_e parallels the shrinking of the exciton wave function size r_{exc} with increasing N concentration. A similar study performed in $GaAs_{1-y}N_y$ quantum wells QWs with $y \sim (1.0–2.0)\%$ shows that m_e remains nearly constant over this y's range. Finally, we consider the magneto-PL properties of $In_xGa_{1-x}As_{1-y}N_y$/GaAs QWs, having $x \sim 30\%$ and $y = (0.7–5.2)\%$. For these samples, the electron effective mass increases with y up to a N concentration equal to 1%, namely, one order of magnitude higher than that found in In-free samples. In the last section, we draw the conclusions of our work.

7.2. EXPERIMENTAL

The samples considered in this review were grown by different techniques on (001)-oriented GaAs substrates. One set of samples consists of four 0.5 μm-thick $GaAs_{1-y}N_y$ epilayers ($y = 0.043$, 0.1, 0.21, 0.5%) grown by metalorganic vapor phase epitaxy [7]. From the same source we studied $GaAs_{1-y}N_y$/GaAs multiple QWs (number of wells equal to three) having thickness $L = 20$ nm and $y = 1.1$, 1.4, and 1.8%. Another set of samples was grown by solid source molecular beam epitaxy and consists of 300 nm-thick $GaAs_{1-y}N_y$ epilayers having $y = 0\%$ and $y < 0.01\%$, and $In_xGa_{1-x}As_{1-y}N_y$/GaAs single quantum wells having $x = (25–42)\%$ and $x = 0\%$, $y = (0.7–5.2)\%$, and QW thickness $L = (6.0–8.2)$ nm. In all cases, sample composition and layer thickness were determined by X-ray diffraction measurements. A $GaAs_{1-y}N_y$ epilayer with $y = 0.1\%$ was hydrogenated at 300°C by a low-energy ion gun (beam energy ~100 eV) in order to vary finely the effective N concentration into the sample [40–49]. PL measurements were carried out in a liquid He optical cryostat for T ranging from 10 to 200 K. The magnetic field was applied parallel to the growth axis of the samples. PL was excited by the 515 nm line of an Ar^+ laser or the 532 nm line of a vanadate-YAG laser, dispersed by a double 3/4 m monochromator, and detected by a N-cooled Ge detector or by a N-cooled InGaAs linear array.

7.3. SINGLE CARRIER LOCALIZATION IN $In_xGa_{1-x}As_{1-y}N_y$

We now address the localization degree of carriers involved in recombination processes at low temperatures in $In_xGa_{1-x}As_{1-y}N_y$ by studying the effect of temperature on magneto-PL.

Recombination from localized states generally dominates emission processes at low temperatures in semiconductor alloys [59–62]. Local fluctuations in the composition lead to an exponential tail of localized states within the crystal forbidden gap [59,63]. The preferential occupancy of these low-energy states by carriers at low T is responsible for asymmetric photoluminescence spectra [11,17,34,35,60,62,64,65], a blue shift of the PL peak energy as the excitation power increases [11,12,34–36,65], a decreasing emission decay time of PL with increasing emission energy [15,17,34,35,37,62], and for an anomalous dependence of the PL maximum energy on temperature [11,15,35,36,62]. All these effects are particularly important in $In_xGa_{1-x}As_{1-y}N_y$. Figure 7.1(a) shows the PL spectra at $T = 50$ K as a function of the laser power, P, of a QW with $x = 0.25$, $y = 0.011$, and $L = 6.0$ nm. At low P, the PL line shape shows a double-peaked structure. The band at lower energy is characterized by a long low-energy tail due to localized states (LS). The higher energy band in Figure 7.1(a) is due to free exciton (or free states, FS) recombination in the $In_xGa_{1-x}As_{1-y}N_y$ quantum well, instead. Similar features were found in other $In_xGa_{1-x}As_{1-y}N_y$ QWs and epilayers [7,10,35,66] and in a large variety of semiconductor

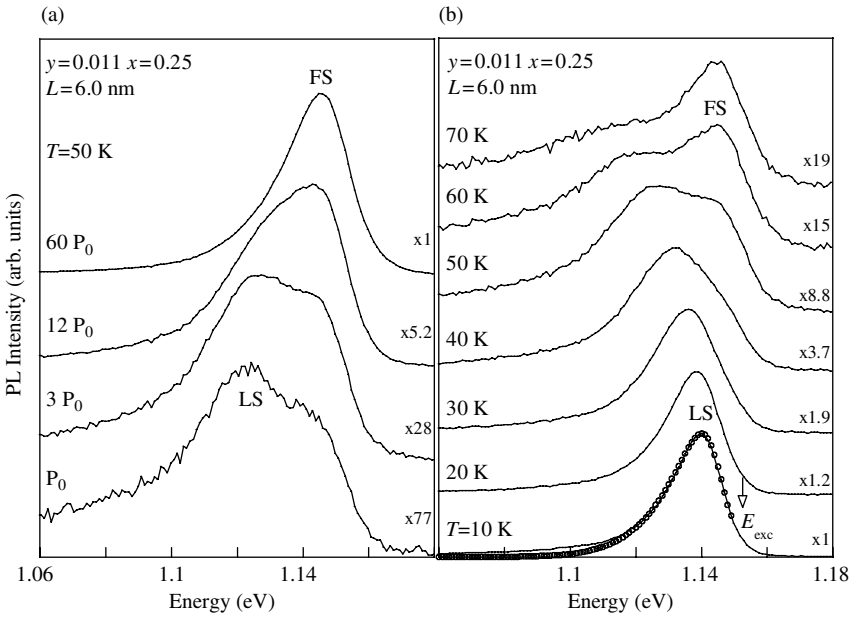

Figure 7.1. (a) Photoluminescence spectra recorded on a $In_xGa_{1-x}As_{1-y}N_y$ quantum well for different laser power intensities ($P_0 = 1.2$ W/cm^2). FS and LS indicate free and localized states, respectively. PL multiplication factors are given. (b) Photoluminescence spectra recorded on a $In_xGa_{1-x}As_{1-y}N_y$ quantum well for different temperatures ($P_0 = 3.3$ W/cm^2). FS and LS indicate free and localized states, respectively. PL multiplication factors are given. The open circles represent the result of a simulation through Eq. (7.2). E_{exc} indicates the energy position of the free exciton state. The spectra are normalized to their peak intensity.

alloys [60,61,67]. The origin of the LS band was attributed to excitons localized on In–N clusters in $In_xGa_{1-x}As_{1-y}N_y$/GaAs heterostructures [7,10] and $InGa_{1-y}N_y$/GaN QWs [67]. For increasing P, the FS band increases its intensity with respect to the LS band due to carrier filling of the localized states. Eventually, at the highest power emission the PL spectrum is dominated by the FS band. The presence of localized states can be inferred also from the temperature dependence of the PL spectra shown in Figure 7.1(b). In fact, with increasing T localized carriers are thermally excited out of N-induced potential minima and for $T = 70$ K only free exciton recombination can be detected. Interestingly, the PL lineshape of localized states presents several features common to other semiconductor alloy systems [59–61,64,65]. The lineshape of the LS band can be accounted for by alloy fluctuations [60] which give rise to an exponential density of localized states [59,68,69]

$$g(E) = g_0 \exp\left\{ - [(E_{exc} - E)/E_0]^{3/2} \right\}, \tag{7.1}$$

where E_{exc} is the free exciton energy, E_0 is a characteristic energy and g_0 is a constant. The PL spectrum is then given by [60,61]

$$L(E) \propto g(E)\tau(E)\exp[f(E)]. \tag{7.2}$$

$\tau(E)$ is the carrier radiative lifetime and $\tau^{-1}(E) \propto 1 + \exp\{\delta[E_M - (E_{exc} - E)]\}$, where δ is the inverse of an effective temperature and E_M is the energy at which the radiative recombination probability equals the transfer probability toward deeper states [59]. For $E < E_M$, localized carriers recombine radiatively, whereas, for $E > E_M$, carriers relax to lower energy states $E' < E$. Finally, $f(E; E_0, E_{exc}, \delta; E_M)$ is a function whose expression can be found in Ref. [60]. The open circles superimposed on the PL spectrum at $T = 10$ K are a simulation using $L(E)$ with $\delta = 0.38$ meV^{-1}, $E_{exc} = 1.153$ eV, $E_0 = 21$ meV, and $E_M = 1.145$ eV. The satisfactory agreement between Eq. (7.2) and the experimental PL lineshape confirms that alloy disorder is the main source of carrier localization at low T.

As far as the nature of localized carriers is concerned, it is assumed usually that potential fluctuations arising from composition disorder localize excitons. Very recently this assumption has been questioned for $GaAs_{1-y}N_y$, where the fast rise time ($\sim$ 25 ps) of the PL signal was used to establish that radiative recombination at low temperatures occurs between *localized* electrons and *delocalized* holes [70].

The degree of localization and/or confinement of carriers in semiconductor heterostructures can be investigated suitably through the dependence of carrier energy levels on magnetic field as measured for instance by magneto-PL [71]. Figure 7.2 shows the PL spectra for different B values of the same $In_xGa_{1-x}As_{1-y}N_y$ QW shown in Figure 7.1(a) and (b) (very similar results have been obtained in all N-containing samples). Parts (a) and (b) of Figure 7.2 show the magneto-PL spectra at $T = 30$ and 180 K, respectively. As shown before, at $T = 30$ K the PL lineshape shows a long low-energy tail characteristic of localized state recombination, which is absent at $T = 180$ K where emission is dominated by free excitons [11,12]; see also Figure 7.1. The shift, ΔE_d, of the PL peak energy induced by the magnetic field is shown in Figure 7.3 as a function of B for the two measurement temperatures. Since the highest value of the magnetic energy in these samples is comparable with the exciton binding energy, the high T data have been fitted by using a variational method, which will be detailed in Section 7.4. The model does not fit the low T dependence of ΔE_d on B, which is linear at least for $B > 4$ T. It should be noticed that for any value of B, ΔE_d is higher at low T than at high T (a factor two for $B = 12$ T). This indicates that at low temperatures the recombining electron–hole pair is more loosely bound than an *exciton*, either localized or free. Indeed, the interaction of these electron–hole pairs at low T with a magnetic field results in a perturbation stronger than Coulomb attraction and, therefore, in a greater diamagnetic shift with respect to the exciton case. Before continuing, we point out that (i) ΔE_d is independent of T at high temperatures where free excitons only contribute to PL [72], (ii) ΔE_d measured at low T decreases when very high power densities are employed (namely, when free excitons start

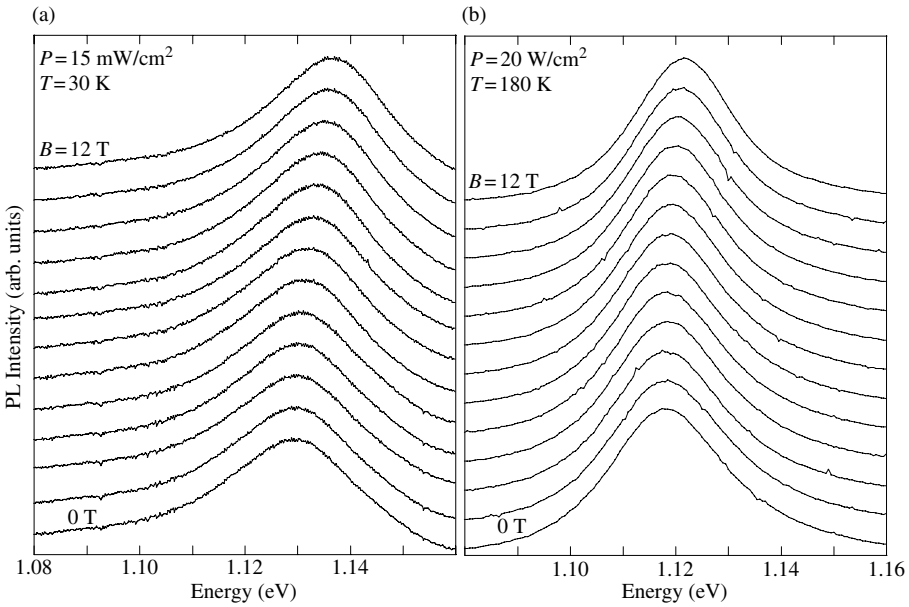

Figure 7.2. (a) Magneto-photoluminescence spectra recorded on a $In_xGa_{1-x}As_{1-y}N_y$ quantum well at $T = 30$ K and laser power density $P = 15$ mW/cm^2. (b) The same as in (a) but $T = 180$ K and $P = 20$ W/cm^2. The spectra are normalized to their peak intensity.

contributing to the PL signal), (iii) these effects are absent in the N-free $In_xGa_{1-x}As$ QWs studied for comparison purposes.

On the basis of these observations, the PL emission at low temperatures can be attributed to recombination of a localized with a delocalized carrier. As for the charge of the localized carriers, one can invoke the model proposed first by Hopfield, Thomas, and Lynch, who suggested that N in GaP is an isoelectronic *electron* trap [73]. Since N in GaAs shares several common features with GaP:N, we argue that N in $In_xGa_{1-x}As$ behaves as an isoelectronic *electron* trap, too. Consequently we argue that the potential minima due to N compositional disorder capture electrons with which *free* holes can recombine, as shown very schematically in the inset of Figure 7.3. Under this hypothesis the electron is strongly localized and the shift of the PL peak with B can be ascribed entirely to the free hole, namely, $\Delta E_d = (e\hbar/2m_h^*)B$ where m_h^* is the hole in-plane effective mass. The continuous line in Figure 7.3 is a fit of this formula to the $T = 30$ K data with $m_h^* = 0.074m_0$ (m_0 is the electron mass in vacuum); as B approaches zero, ΔE_d deviates from a linear behavior likely because of a residual electrostatic interaction between electrons and holes. A somewhat similar approach has been used for deriving the electron effective mass from the B-induced shift of free-electron to neutral-acceptor recombinations [74–82] and will be used in Section 7.4.

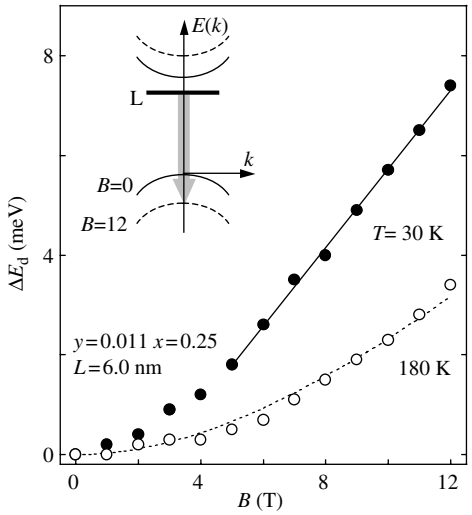

Figure 7.3. Diamagnetic shift, ΔE_d, of the PL peak measured in a 6.0 nm-thick $In_{0.25}Ga_{0.75}As_{0.989}N_{0.011}$ QW at $T = 30$ K (filled dots) and $T = 180$ K (open circles) versus magnetic field, B. The dashed curve is a fit to the $T = 180$ K data by the variational method described in Section 7.4.2. The continuous line is a fit to the $T = 30$ K data ($B > 4$ T) by $\Delta E_d = (e\hbar/2m_h^*)B$, where m_h^* is the in-plane hole effective mass. The inset depicts the recombination at low temperatures occurring in $In_xGa_{1-x}As_{1-y}N_y$ in a reciprocal space scheme at $\mathbf{k} \sim 0$ for $B = 0$ T (continuous parabolas) and $B = 12$ T (dashed parabolas). L indicates the localized levels related to nitrogen. Reprinted with permission from Ref. [82], copyright (2004) by the American Institute of Physics.

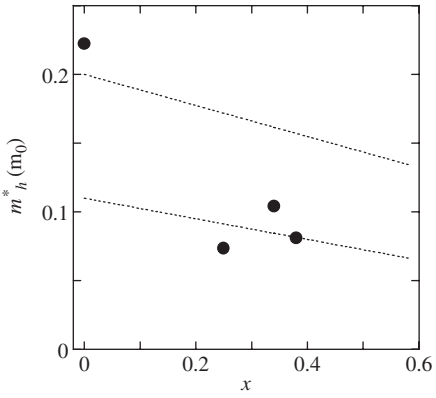

Figure 7.4. Dependence of the in-plane hole effective mass in $In_xGa_{1-x}As_{1-y}N_y$ quantum wells as a function of the In concentration, x. The dashed lines are the values of the in-plane light (upper line) and heavy (lower line) hole, as estimated by using the Luttinger parameters [83]. Reprinted with permission from Ref. [82], copyright (2004) by the American Institute of Physics.

Figure 7.4 shows the m_h^* values derived in $In_xGa_{1-x}As_{1-y}N_y$ QWs as a function of the In concentration. Since N incorporation affects mainly the conduction band states, we compare the m_h^* values derived here with those of the heavy and light hole of the N-free $In_xGa_{1-x}As$ host. In fact, due to the different types of strain, compressive in $In_xGa_{1-x}As_{1-y}N_y$ and tensile in $GaAs_{1-y}N_y$, in-plane heavy and light holes should be considered in the former and latter case. The dashed lines in Figure 7.4 are the $In_xGa_{1-x}As$ in-plane hole masses as estimated through the Luttinger parameters [83]. The good agreement of the experimental data with the hole curves supports our hypothesis about the hole nature of the delocalized carrier.

As a final comment, our results show that a measure of the properties of extended states through magneto-PL needs to be done at temperatures high enough to get rid of localized carrier contributions.

7.4. MEASUREMENT OF THE ELECTRON EFFECTIVE MASS AND EXCITON WAVE FUNCTION SIZE

N incorporation in $In_xGa_{1-x}As$ modifies strongly the electronic properties of the host lattice as it is widely reported in the present book. There is a general consensus that the origin of these modifications is related to the quite strong carrier localization around the N atom, which is produced by the high electronegativity and small size of the N atoms with respect to those of the replaced As atoms. Different models have been proposed to explain the effects N has on the host material. In a first theoretical model, the strong perturbation of the translational symmetry of the host lattice potential due to N incorporation gives rise to perturbed host states [84]. In turn, this leads to a downward shift of the conduction band (CB) minimum (CBM) for increasing N concentration and to a progressive disappearance of the energy levels of N clusters in the bandgap [84]. In a band anticrossing model, instead, a phenomenological repulsive interaction between the CBM and a single N level resonant with the CB continuum of states accounts for most N-related effects [6]. This model has been supported by recent tight-binding calculations [85]. Finally, the effects of the interaction among N atoms and/or clusters and the ensuing impurity-band formation in invoked in a third model [19]. In all the models a decrease in the host bandgap is predicted when the N concentration increases, in quite a good agreement with all the experimental data reported from different groups. The effect of N incorporation on the electron effective mass m_e is more subtle and it may represent a more stringent test for the validity of the different theoretical approaches aimed at explaining the puzzling effects of N in $In_xGa_{1-x}As_{1-y}N_y$. Unfortunately, the experimental data on m_e reported in the literature do not show a common and clear trend with increasing N concentration.

Figure 7.5 shows the values of the electron effective mass as a function of y for different $GaAs_{1-y}N_y$ QWs and epilayers as measured by different groups. A large difference both in the m_e values and trends with y can be observed. The data of Refs. [19,21] were derived

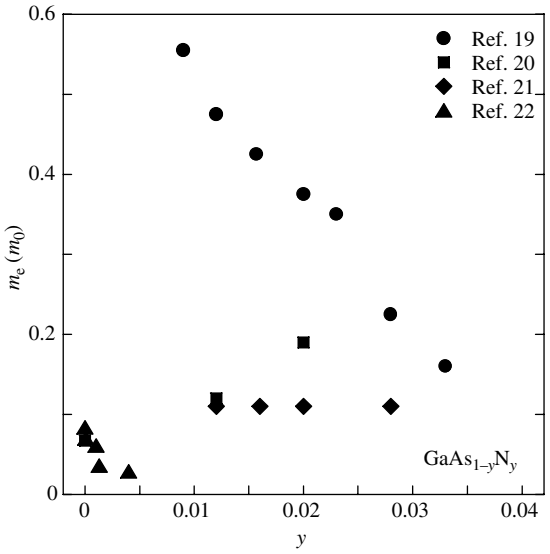

Figure 7.5. $GaAs_{1-y}N_y$ electron effective mass as a function of N concentration as derived from the literature (see figure legend).

from a fit of the transition energies of $GaAs_{1-y}N_y$ QWs within the envelope function approximation, which needs some unknown parameters as the bandgap offsets between $GaAs_{1-y}N_y$ and GaAs. The data of Ref. [19] show a continuous decrease in m_e with y, which supports the impurity-band formation model proposed therein. On the contrary, in the same N concentration interval, the m_e values reported in Ref. [21] are very different and do not change sizably with y. The data of Ref. [22] were determined by combining four different transport measurements and display a decrease in m_e when y increases. This behavior was justified within a **k·p** approach [22]. A more direct measurement of m_e was used by Hai and coworkers through optically detected cyclotron resonance measurements [20]. In this case m_e increases linearly with y.

The data of electron effective mass reported in the literature for $In_xGa_{1-x}As_{1-y}N_y$ alloys display a less scattered distribution with respect to the $GaAs_{1-y}N_y$ case. This is shown in Figure 7.6. Most of the m_e data were derived from a fit of the $In_xGa_{1-x}As_{1-y}N_y$ QW transition energies using the electron effective mass as one of the fitting parameters [25–27, 29,30]. A combination of infrared reflectivity and Hall measurements were employed in Ref. [28], whereas electron energy loss measurements were reported in Ref. [31]. For $In_xGa_{1-x}As_{1-y}N_y$ a rather common behavior can be deduced from the experimental data reported. m_e increases with increasing y and it tends to saturation for $y > 1.0\%$.

We now present the data on the electron effective mass and exciton size determined by us through magneto-PL measurements.

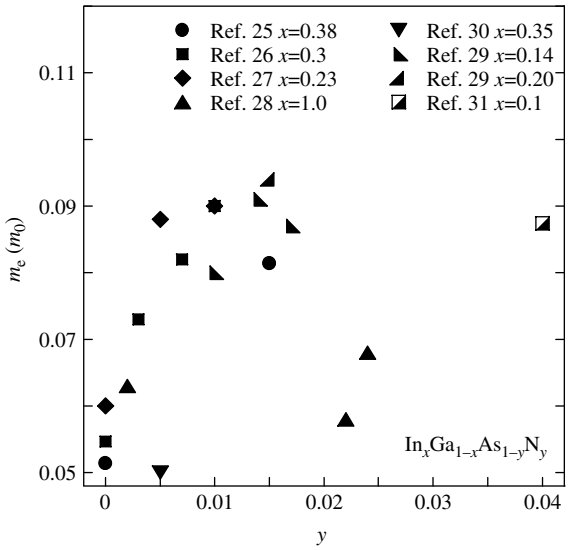

Figure 7.6. $In_xGa_{1-x}As_{1-y}N_y$ electron effective mass as a function of N concentration as derived from the literature (see figure legend, where different In concentration values are reported).

7.4.1 $GaAs_{1-y}N_y$

We describe briefly the PL properties of the investigated samples.

Figure 7.7 shows the PL spectra of a set of $GaAs_{1-y}N_y$ epilayers having different N concentration. At the very early stage of N incorporation in GaAs (N concentration lower than 0.01%, bottommost curve in Figure 7.7), the PL spectrum is characterized by a number of sharp lines (linewidth ~0.5 meV) between 1.40 and 1.48 eV. These lines are attributed to carrier recombination from electronic levels due to N pairs and/or clusters [86–91] and are superimposed on a broad band also related to N incorporation. The luminescence intensity of these transitions varies from line to line and increases with y (not shown here). An exact assignment of each line to a given N complex is made rather difficult by the strong dependence of the material optical properties on the growth conditions, as extensively reported in the literature [87,89–91]. Free-electron to neutral-carbon acceptor, (e, C), and free-exciton, E_-, recombinations are observed at 1.493 and 1.515 eV, respectively. As the nitrogen concentration is increased further ($y = 0.043$ and 0.1%), the energy of the excitonic recombination from the material's bandgap E_- as well as the (e, C) recombination band start red shifting very rapidly, thus coexisting with and taking in the levels associated with the N complexes. The energy of these levels does not change with N concentration [7,89,90]. These features highlight the strongly localized character of the N isoelectronic traps, contrary to that of shallow impurities whose wave functions overlap at smaller concentrations (10^{16}–10^{18} cm^{-3}). Eventually at higher N

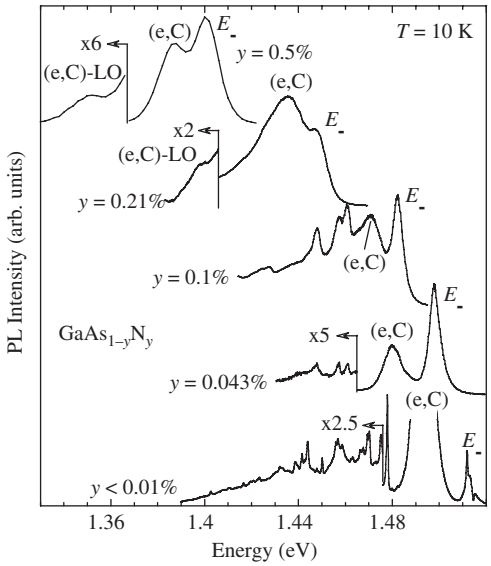

Figure 7.7. Peak-normalized low-temperature (10 K) photoluminescence spectra of $GaAs_{1-y}N_y$ epilayers with different *y*s. E_- and (e, C) indicate the free-exciton and free-electron to neutral-carbon acceptor recombination, respectively. (e, C)-LO indicates the longitudinal optical phonon replica of the (e, C) transition.

concentrations (alloy limit, $y > 0.1\%$) the $GaAs_{1-y}N_y$ bandgap keeps red shifting [92] along with the C-related states [89].

Figure 7.8 shows the PL spectra of another set of $GaAs_{1-y}N_y$ samples (from the same source of the samples shown in Figure 7.7) consisting of $GaAs_{1-y}N_y$/GaAs 20 nm-thick quantum wells. The data have been recorded at a temperature and laser power so as to highlight the contribution of the free-electron to neutral-carbon acceptor (and its LO phonon replica) recombination in the $GaAs_{1-y}N_y$ well. The contribution of the free-exciton is also indicated in the spectra. We point out that at lower *P* and *T* the contribution from localized states becomes predominant and we have not considered these experimental conditions when performing magneto-PL measurements.

The presence of the (e, C) transitions in our samples plays an important role in the determination of the electron effective mass as it will be shown in the following.

Figure 7.9(a) and (b) shows the PL spectra recorded under different *B* values for $GaAs_{1-y}N_y$ epilayers having $y = 0.043$ and 0.1%, respectively. In both the samples, the E_- and (e, C) peak energies blue shift upon application of *B* at a rate decreasing with increasing N concentration. On the contrary, the emission lines located below the (e, C) band and due to carrier recombination on N complexes remain fixed as *B* increases, according to the strongly localized character N pairs and clusters have. The different

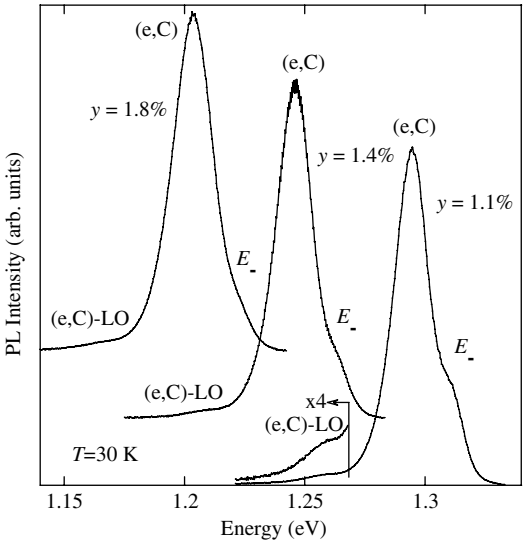

Figure 7.8. Peak-normalized low-temperature (30 K) photoluminescence spectra of 20 nm-thick $GaAs_{1-y}N_y$ quantum wells with different ys. E_- and (e, C) indicate the free-exciton and free-electron to neutral-carbon acceptor recombinations, respectively. (e, C)-LO indicates the longitudinal optical phonon replica of the (e, C) transition.

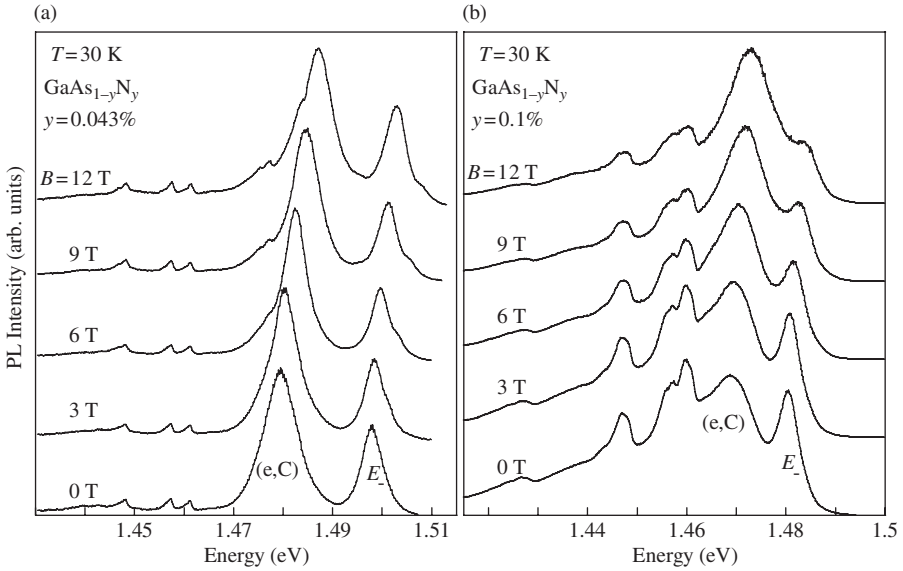

Figure 7.9. (a) Peak-normalized photoluminescence spectra of a $GaAs_{1-y}N_y$ epilayer with $y = 0.043\%$ taken at different magnetic fields ($T \sim 30$ K). E_- and (e, C) indicate the free-exciton and free-electron to neutral-carbon acceptor recombinations, respectively. (b) Same as in (a) but $y = 0.1\%$. Reprinted with permission from Ref. [81], copyright (2003) by the American Institute of Physics.

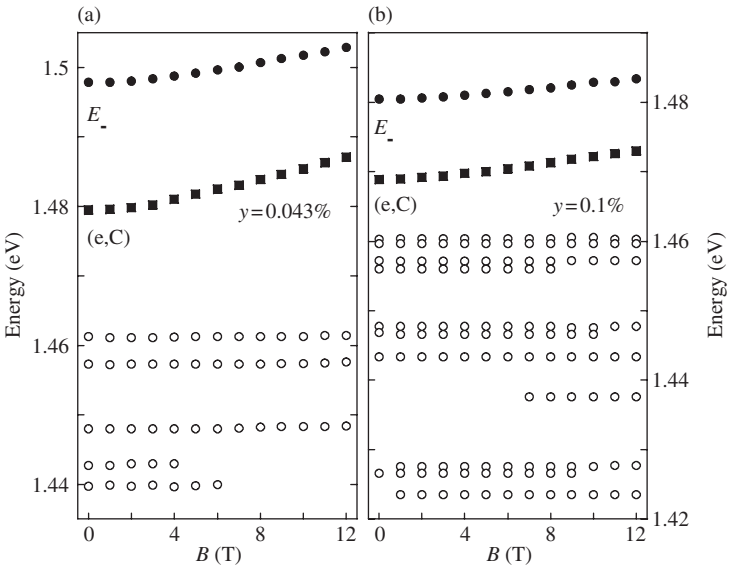

Figure 7.10. (a) B dependence of the peak energy of the different recombination bands observed in Figure 7.9(a). (b) B dependence of the peak energy of the different recombination bands observed in Figure 7.9(b). Note that only the (e, C) and E_- transitions display a sizable shift with B.

behavior of localized and extended states can be best observed in Figure 7.10(a) and (b), which shows the dependence of the peak energy of each PL emission on magnetic field for the same samples of Figure 7.9. In particular, the E_- band shifts with B at a lower rate than the (e, C) band, owing to the larger Coulomb attraction between the electron and hole in the former case. A qualitatively similar finding is observed in $GaAs_{1-y}N_y$/GaAs quantum wells. Figure 7.11 shows the PL spectra recorded at different B values for a 20 nm-thick $GaAs_{1-y}N_y$/GaAs QW sample. As shown in Figure 7.8, free-electron to neutral-carbon recombination is the most intense feature in the PL spectra.

We exploit the (e, C) energy shift to derive the electron effective mass in $GaAs_{1-y}N_y$ for different N concentrations as explained in the following. Figure 7.12 sketches the E_- and (e, C) recombinations in a reciprocal space scheme at $\mathbf{k} \sim 0$. Following the arguments first invoked by Rossi, Wolfe, and Dimmock [74] and followed by many other authors [75–82], the C-related level stays fixed in energy because of the dispersion-less characteristics (i.e. infinite effective mass) of the C impurity level in $\mathbf{k}$-space. On the contrary, the conduction band bottom and the valence band top shift upon application of B. Therefore, in this approximation the shift of the (e, C) transition is ascribed entirely to the shift of the first Landau electron level associated with the conduction band bottom. Figures 7.13 and 7.14 show the B-induced diamagnetic shift, $\Delta E_d = E(B) - E(0)$, of the (e, C) recombination band for different N concentrations; the data are offset vertically for

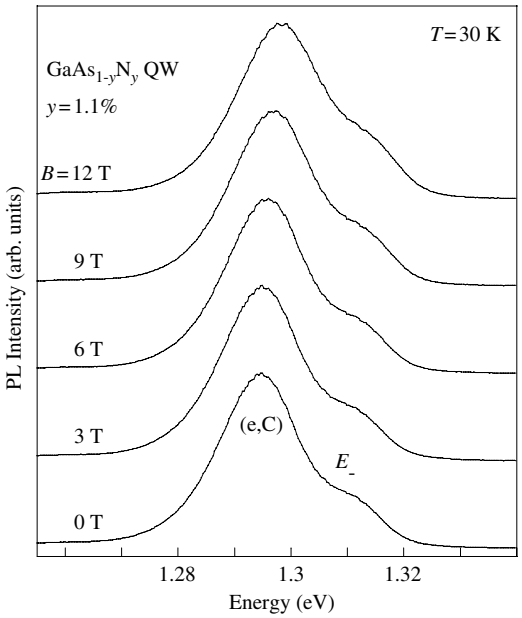

Figure 7.11. Peak-normalized photoluminescence spectra ($T = 30$ K) recorded at different magnetic fields for a $GaAs_{1-y}N_y$ quantum well with $y = 1.1\%$. E_- and (e, C) indicate the free-exciton and free-electron to neutral-carbon acceptor recombinations, respectively.

ease of comparison. The dashed lines are a fit to the data by means of the formula for the magnetic field dependence of the bottommost Landau level of the conduction band, i.e. $\Delta E_d = sB = (\hbar e/2m_e)B$. The slope s of the shift of the (e, C) transition in the B-linear region of ΔE_d provides *directly* the value of the electron effective mass. Note that at zero magnetic field, ΔE_d extrapolates to a negative value, of order of $k_B T/2$, as found in other magneto-PL measurements of the B-induced shift of free-electron to neutral-acceptor

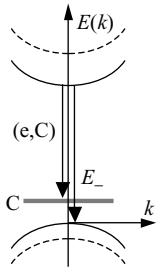

Figure 7.12. Sketch of the free-exciton (E_-) and free-electron to neutral-carbon acceptor [(e, C)] recombinations in a reciprocal space scheme at $\boldsymbol{k} \sim 0$ for $B = 0$ T (continuous parabolas) and $B = 12$ T (dashed parabolas). C indicates the dispertion-less carbon level in the reciprocal space.

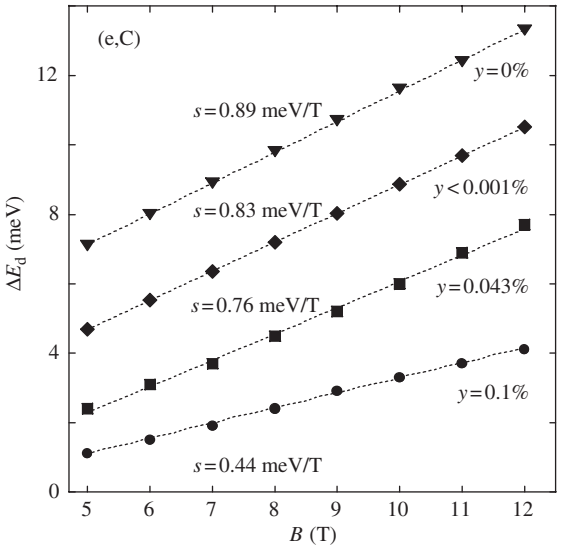

Figure 7.13. *B*-induced shift value, ΔE_d, of the (e, C) peak energy as a function of the magnetic field for different $GaAs_{1-y}N_y$ epilayers. The continuous lines are fits to the data by $\Delta E_d = (\hbar e/2m_e)B$. The electron effective mass m_e is derived directly from the line slope s, also shown in the figure. The data for $y = 0\%$ are offset by 4.0 meV, for $y < 0.001\%$ by 1.5 meV, for $y = 0.043\%$ by 0.1 meV for ease of comparison.

recombinations [75–80]. This behavior is usually attributed to the change in the density of states of the system from three- to one-dimensional due to the applied magnetic field. In addition, a residual Coulomb attraction between the CB electron and the hole localized on the C acceptor may be responsible for a non-linear behavior at low B values.

Figure 7.15 shows the dependence of the electron effective mass on N concentration. Circles and squares refer to $GaAs_{1-y}N_y$ epilayers and quantum wells, respectively. Two main features can be observed. First, the m_e values show a steep increase already for $y \sim 0.1\%$ within a very narrow concentration interval. Second, the electron effective mass does not change much from $y \sim 0.1$ up to $\sim 2\%$. We comment briefly on the first finding. Figure 7.7 shows that when increasing y the CB minimum red shifts rapidly while the N-related cluster states (CS) remain pinned in energy. Furthermore, for $y \sim 0.1\%$ the CB minimum crosses the CS and concomitantly the electron effective mass increases suddenly. Such an increase can be attributed to a strong interaction between N-complex states and the states of the CB minimum. The role of CS was invoked as essential for accounting for the electronic properties of dilute nitrides, in particular the bandgap reduction [45], and it has been taken into account very recently for explaining the data shown in Figure 7.15 [93]. We have to mention that a band anticrossing model [6,85] provides a means to calculate the electron effective mass. However, this model

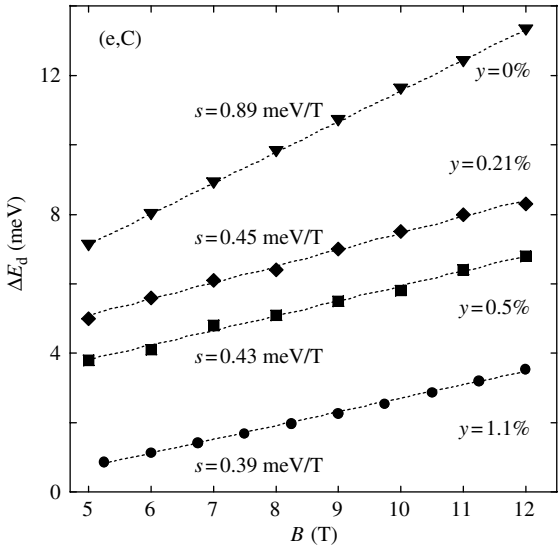

Figure 7.14. B-induced shift value, ΔE_d, of the (e, C) peak energy as a function of the magnetic field for different $GaAs_{1-y}N_y$ epilayers and a quantum well ($y = 1.1\%$, circles). The continuous lines are fits to the data by $\Delta E_d = (\hbar e/2m_e)B$. The electron effective mass m_e is derived directly from the line slope s, also shown in the figure. The data for $y = 0\%$ are offset by 4.0 meV, for $y = 0.21\%$ by 4.0 meV, for $y = 0.50\%$ by 1.5 meV for ease of comparison.

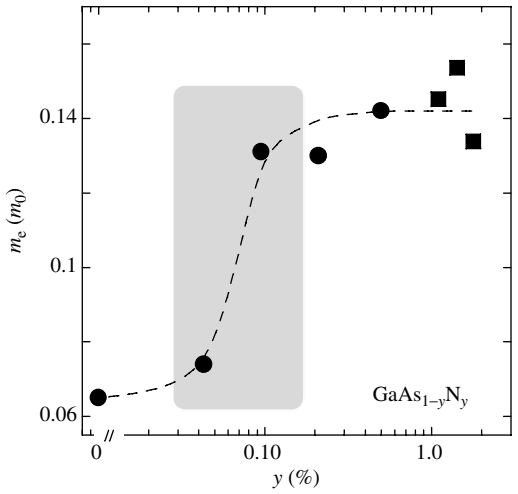

Figure 7.15. Electron effective mass versus N concentration for $GaAs_{1-y}N_y$ epilayers (circles) and quantum wells (squares). The gray area highlights the concentration interval where the electron effective mass varies most. The dashed line is a guide to the eye. Reprinted with permission from Ref. [81], copyright (2003) by the American Institute of Physics.

underestimates the electron effective mass increase, at least for reasonable values of the interaction potential.

In order to follow closely the variation of m_e with the N effective concentration, we performed a study similar to that described above in a sample irradiated at different H doses. As already reported by us, H tunes in a controllable and reversible way the electronic properties of $In_xGa_{1-x}As_{1-y}N_y$ and $GaP_{1-y}N_y$ [40–49]. This is illustrated in Figure 7.16 for a $GaAs_{1-y}N_y$ epilayer ($y = 0.1\%$). H irradiation leads first to a passivation of the N cluster states (see second curve from bottom) and then to an apparent reopening of the $GaAs_{1-y}N_y$ bandgap toward that of the GaAs reference (topmost continuous curve). As a matter of fact, both the (e, C) and the E_- recombination bands converge to those of the GaAs reference with increasing H dose, as shown by continuous lines in Figure 7.16.

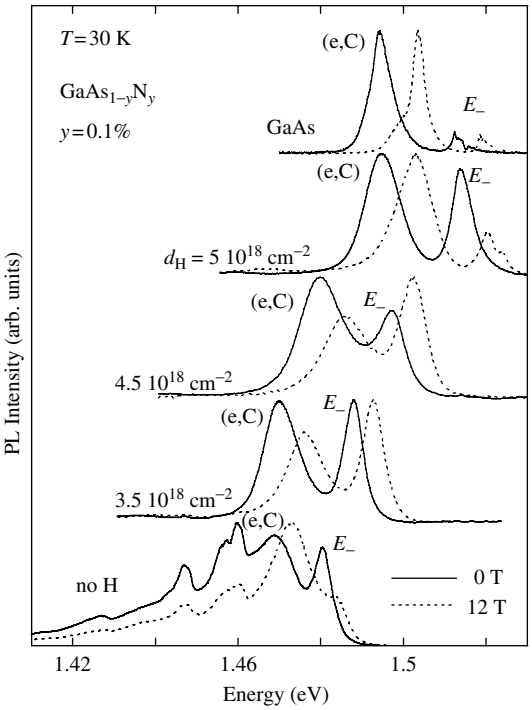

Figure 7.16. Peak-normalized photoluminescence spectra of a $GaAs_{0.999}N_{0.001}$ alloy treated with different hydrogen doses d_H. Measurements have been performed at about $T = 30$ K to reduce the contribution from possible N-related localized states and donor-acceptor pair recombination. The bottommost and topmost spectra refer to an untreated $GaAs_{1-y}N_y$ and a reference GaAs sample, respectively. Continuous and dashed lines indicate PL spectra taken under zero and 12 T magnetic field, respectively. (e, C) indicates the free-electron to neutral-carbon recombination and E_- indicates the free-exciton recombination. Different laser power densities have been employed for the different samples in order to highlight the presence of both (e, C) and E_- bands. Reprinted with permission from Ref. [49], copyright (2004) by the American Physical Society.

With applying a magnetic field (dashed curves in Figure 7.15), the E_- and (e, C) bands blue shift with increasing B. Notice that the energy separation between these two transitions increases on going from the H-free to the H-treated samples, due to a corresponding decrease in the tensile strain with decreasing the effective N concentration [48]. In fact, for decreasing N concentration the top of the valence band acquires a more pronounced heavy-hole character and, in turn, the binding energy of the acceptor impurity increases.

In Figure 7.17, the energy shift, ΔE_d, of the (e, C) recombination lines are shown as a function of B for $GaAs_{1-y}N_y$ (both untreated and hydrogenated) and for the GaAs reference. The same analysis performed for the untreated samples (see Figures 7.13 and 7.14) has been applied to the hydrogenated samples. We point out that the slope s of the lines fitting the (e, C) transitions increases with increasing H dose until the slope of the GaAs reference is obtained.

Figure 7.18 shows the electron effective mass as a function of the energy of the band-gap exciton. Note that a sound value of m_e ($= 0.065m_0$, where m_0 is the electron mass in the vacuum) is obtained for the GaAs reference with this method. Filled circles refer to the $GaAs_{1-y}N_y$ alloy with $y = 0.1\%$ for both the untreated sample (gray symbol) and the

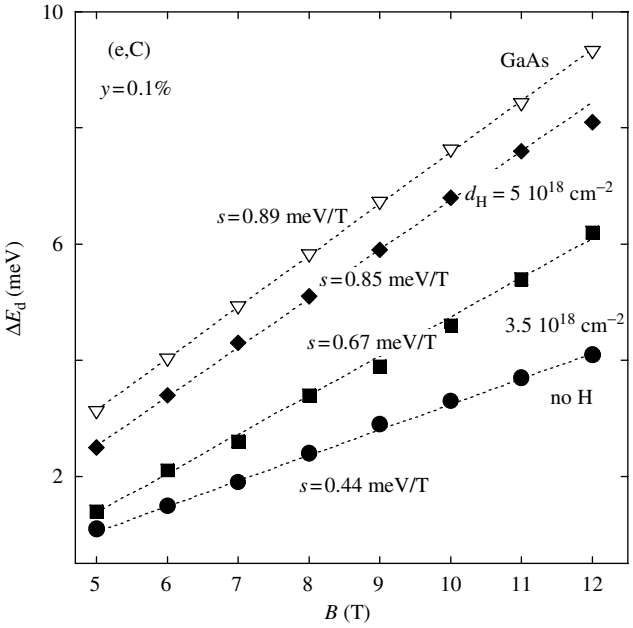

Figure 7.17. B-induced shift value, ΔE_d, of the (e, C) peak energy as a function of the magnetic field for different $GaAs_{1-y}N_y$ epilayers. The continuous lines are fits of $\Delta E_d = (\hbar e/2m_e)B$ to the data. The electron effective mass m_e is derived directly from the line slope s, also shown in the figure.

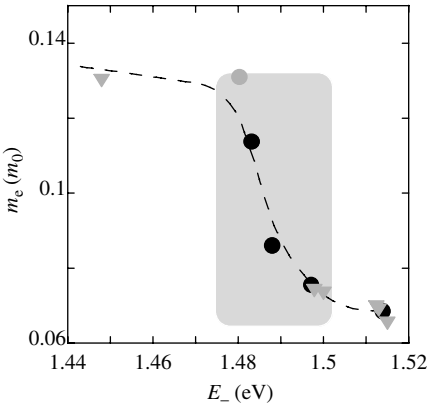

Figure 7.18. Dependence of the electron effective mass on the free-exciton peak energy at 10 K. Filled dots refer to the untreated (gray) and hydrogenated (black) $GaAs_{0.999}N_{0.001}$ samples, gray triangles refer to $GaAs_{1-y}N_y$ alloys with different y values (both untreated and irradiated with H). The gray area highlights the concentration interval where the electron effective mass varies most (see also Figure 7.15). The dashed line is a guide to the eye. Reprinted with permission from Ref. [49], copyright (2004) by the American Physical Society.

hydrogenated samples (black symbols). Gray filled triangles are the m_e values measured in unhydrogenated samples with different N concentration ($y = 0$, $y < 0.01\%$, $y = 0.043$, and 0.21% both untreated and H-irradiated). m_e varies biuniquely with the sample bandgap energy, namely, it depends on the *effective* N concentration in the crystal regardless of how this concentration has been achieved (either by N incorporation in GaAs or by H irradiation of $GaAs_{1-y}N_y$). Most importantly, these findings allow monitoring the evolution of the electronic properties of $GaAs_{1-y}N_y$ in a virtually continuous manner. In particular, the sudden change in m_e shown in Figure 7.15 is confirmed, thus providing further evidence that N-induced localization effects start at very low values of y. Interestingly, the energy at which the electron effective mass increases abruptly (~ 1.485 eV) falls in a spectral region where many N-related complexes emit [7,86–91]. In particular, a cluster emitting at 1.478 eV can be observed in the bottommost spectrum of Figure 7.7 ($y < 0.01\%$). In turn, the interaction between this cluster (or others falling in a nearby energy interval) might be responsible for the large variation in m_e.

Theoretical calculations predict that the electron wave function at the conduction band edge E_- has a given percentage of non-Γ character because of translation symmetry breaking of the lattice stemming from N incorporation [89,94]. This results in a sizeable wave function localization despite the fact that the E_- state has an extended character far away from nitrogen [84,94]. Such localization affects the electron effective mass as well as the exciton wave function size. Magneto-PL can be used to estimate the average spatial extent of bound-carrier systems [95]. Several theories and calculation techniques have

been developed to study the properties of magnetoexcitons in semiconductors [96–101]. The simultaneous effect of the Coulomb interaction and an external magnetic field on an electron–hole bound system is a difficult problem, which often can be solved only under specific magnetic field limits. For excitons in bulk $GaAs_{1-y}N_y$ we restrict ourselves to magnetic fields low enough to treat B as a perturbation [95].

Figure 7.19 shows the dependence of the exciton diamagnetic shift on B for different N concentrations. The continuous lines are fits of $\Delta E_d = \alpha B^2 = e^2\langle r_{eh}^2\rangle/(8\mu)B^2$ to the exciton diamagnetic shift in the low-field regime (small perturbation limit [95]). r_{eh} and μ are, respectively, the electron–hole distance and the reduced effective mass of excitons. At very low N concentration, α rapidly decreases by a factor of ~ 2 with respect to the value it has in GaAs and tends to saturate for $y > 0.1\%$ (not shown here). This behavior matches well with that found for m_e. By using the m_e values determined previously, we get an estimate of $r_{exc} = \sqrt{\langle r_{eh}^2\rangle}$ for each sample from the diamagnetic shift formula $\Delta E_d = \alpha B^2$. The r_{exc} values are shown as a function of y in the inset of Figure 7.19. The fast decrease in r_{exc} provides further evidence that N-induced localization effects start at very low values of y.

We performed a similar study in hydrogenated $GaAs_{1-y}N_y$ epilayers. Figure 7.20 shows the shift ΔE_d of the exciton energy as a function of B^2 for $GaAs_{1-y}N_y$ with $y = 0.1\%$ (both untreated and hydrogenated, filled symbols) and for the GaAs reference (open symbols). The continuous lines are a fit of $\Delta E_d = [e^2\langle r_{eh}^2\rangle/(8\mu)]B^2$ to the E_- data in the quadratic low-field region similar to what shown in Figure 7.19. The inset of Figure 7.20 shows in

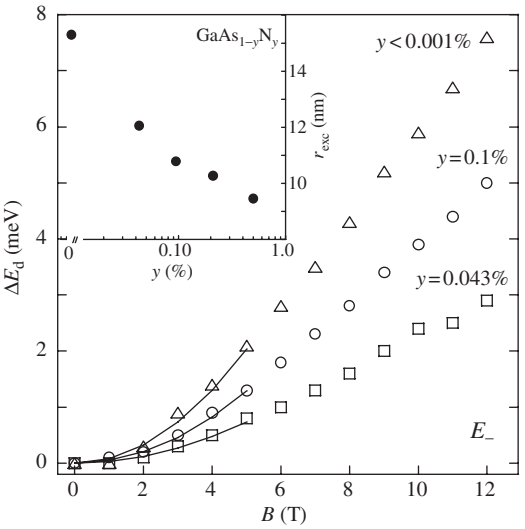

Figure 7.19. Energy shift with magnetic field of the free-exciton recombination E_- for different $GaAs_{1-y}N_y$ epilayers. The continuous lines are fits of $\Delta E_d = [e^2\langle r_{eh}^2\rangle/(8\mu)]B^2$ to the data, where $\langle r_{eh}^2\rangle$ is a fit parameter. The inset shows the dependence of $r_{exc} = \sqrt{\langle r_{eh}^2\rangle}$ on N concentration.

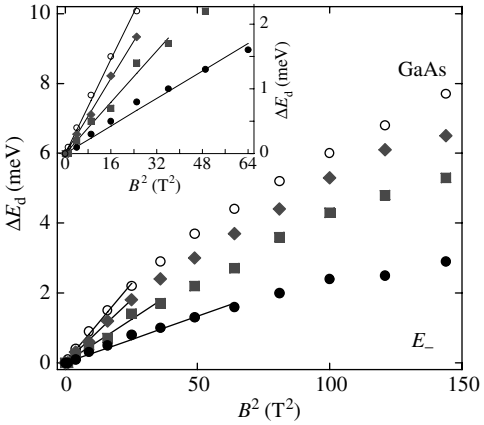

Figure 7.20. Energy shift with B^2 of the free-exciton recombination E_- for a $GaAs_{0.999}N_{0.001}$ epilayer. Black symbols refer to the untreated sample, gray symbols refer to hydrogenated samples, and open symbols refer to a GaAs reference. The continuous lines in the inset are fits of $\Delta E_d = [e^2\langle r_{eh}^2\rangle/(8\mu)]B^2$ to the data. $\langle r_{eh}^2\rangle$ is the only fit parameter.

detail the B range where a B^2 approximation holds. Figure 7.21 shows the dependence of the exciton size on the exciton bandgap energy. Symbols have the same meaning as in Figure 7.18. Similar to m_e, the combined use of untreated and H-irradiated samples allows us to follow the evolution of the electronic properties of carriers in $GaAs_{1-y}N_y$ in detail, thus providing firm guidelines to models aimed at describing the electronic properties of dilute nitrides.

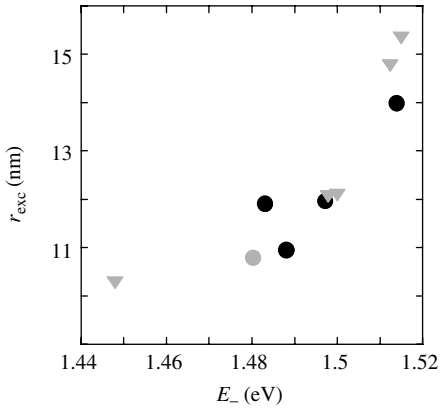

Figure 7.21. Exciton size dependence on the free-exciton peak energy at 10 K. Filled dots refer to the untreated (gray) and hydrogenated (black) $GaAs_{0.999}N_{0.001}$ sample, gray triangles refer to $GaAs_{1-y}N_y$ alloys with different y values. Reprinted with permission from Ref. [49], copyright (2004) by the American Physical Society.

7.4.2 $In_xGa_{1-x}As_{1-y}N_y$

$In_xGa_{1-x}As_{1-y}N_y$ alloys present several interesting features. Indeed, a preferential formation of In-N over Ga-N bonds in annealed $In_xGa_{1-x}As_{1-y}N_y$ was reported in Refs. [102,103] by using bandgap and vibrational mode measurements, respectively. Strain reduction was proposed as the driving mechanisms leading to an In-rich environment of the N atoms [102,103]. Monte Carlo simulations confirmed the experimental findings [104], although recent X-ray absorption measurements showed a much reduced effect of short-range ordering [105]. Another important feature of $In_xGa_{1-x}As_{1-y}N_y$ is the variation of the relative energy distance between the levels introduced by N atoms and the CBM of the host matrix due to In alloying. A slower rate in the bandgap reduction upon N incorporation is usually observed in $In_xGa_{1-x}As_{1-y}N_y$ with respect to $GaAs_{1-y}N_y$ [1–4]. Also, the rate at which the bandgap depends on temperature as compared with the N-free lattice shows a smaller variation in In-containing than in In-free nitrides [11,12]. We now consider the effect of N on the electron effective mass of $In_xGa_{1-x}As$ alloys with high x (~30%).

Figure 7.22(a) and (b) shows the magneto-PL spectra at $T = 100$ K of 6.0 nm-thick $In_{0.32}Ga_{0.68}As_{1-y}N_y$ QWs having $y = 0$ and 2.7%, respectively. The data were recorded at a temperature high enough as to have no emission contribution from

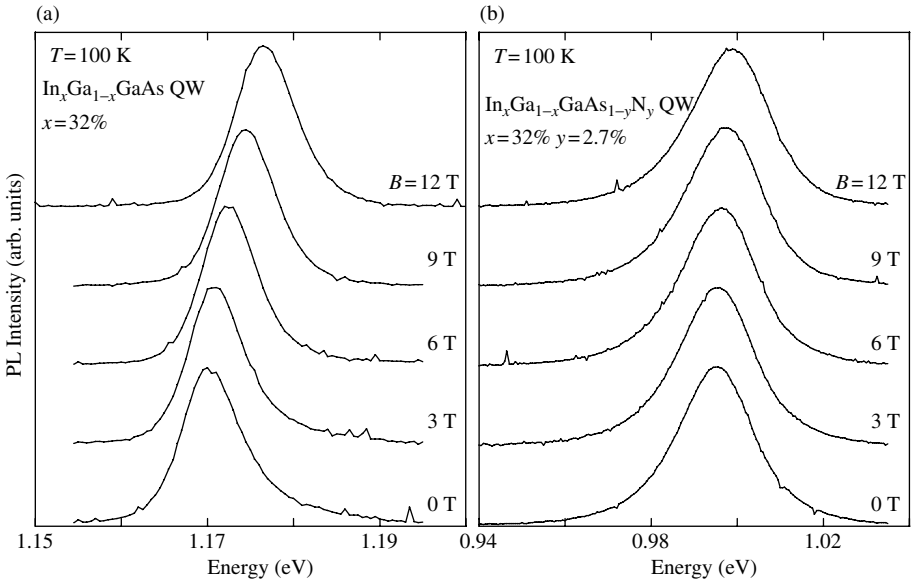

Figure 7.22. (a) Peak-normalized photoluminescence spectra recorded at $T = 100$ K and different magnetic fields for a 6 nm-thick $In_{0.32}Ga_{0.68}As_{1-y}N_y$ QWs having $y = 0\%$. (b) Same as in (a) but $y = 2.7\%$.

localized carriers. The N-containing sample shows a smaller diamagnetic shift consistent with a heavier reduced mass and smaller wave function extent of exciton.

Since carriers in present samples have an enhanced two-dimensional character because of the strong confining potential provided by the high In concentration ($x \sim 0.3$) in the QWs, we analyze the diamagnetic shift of the exciton by considering a variational method in two dimensions. We use the exciton effective mass (μ) as an adjustable parameter [100,101]. The Hamiltonian of the system is given by

$$H_\rho = -\frac{\partial^2}{\partial\rho^2} - \frac{1}{\rho}\frac{\partial}{\partial\rho} + \frac{\gamma^2\rho^2}{4} - \frac{2}{\rho}. \tag{7.3}$$

ρ is the exciton radial coordinate in the QW plane,

$$\gamma = \frac{eB\hbar}{2\mu\mathrm{Ry}}$$

Ry is the exciton binding energy

$$\mathrm{Ry} = \frac{e^2}{8\pi\varepsilon a_0},$$

where ε is the absolute dielectric constant of the host lattice and

$$a_0 = \frac{4\pi\varepsilon\hbar^2}{\mu e^2}$$

is the exciton Bohr radius. The $-2/\rho$ term in the right-hand side of Eq. (7.3) represents the Coulomb potential [99,100]. The value of μ is found by rendering minimum the expectation value of H_ρ calculated over the trial wave function of the exciton given by [101]

$$\phi(\rho, \lambda, \sigma) = \exp\left(-\frac{\gamma\rho^2}{4\sigma} - 2\lambda\rho\right), \tag{7.4}$$

where λ and σ are two variational parameters.

Figure 7.23 shows the result of the fitting procedure applied to the experimental diamagnetic shift values for the two QWs shown in Figure 7.22. The exciton effective mass values are $\mu = 0.039m_0$ and $0.049m_0$ for $y = 0$ and 2.7%, respectively. In order to derive the electron effective mass from our data we set the in-plane effective mass of holes equal to $0.11m_0$ in agreement with the data reported in Ref. [106] and shown in Figure 7.4 of Section 7.3. Figure 7.24 shows the dependence of m_e (filled symbols) on N concentration. Data derived from the literature are also shown (open symbols) for comparison purposes. A good agreement is found between our results and those obtained by different experimental techniques. This is in contrast with the scattered values of m_e reported by various authors in $GaAs_{1-y}N_y$ (see Figure 7.5).

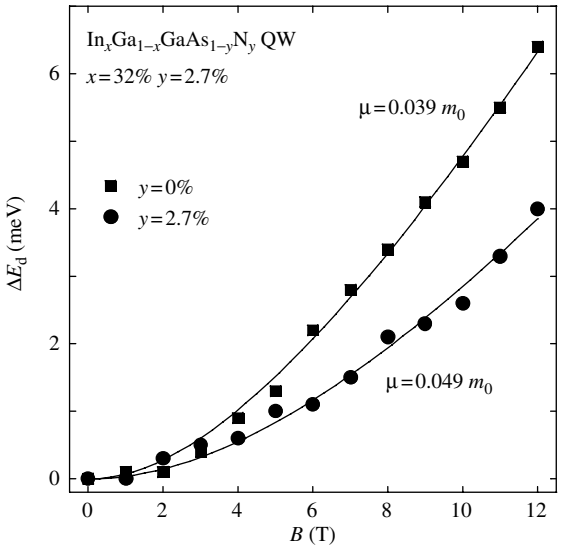

Figure 7.23. Diamagnetic shift, ΔE_d, measured at $T = 100$ K in an $In_{0.32}Ga_{0.68}As_{0.973}N_{0.027}$ QW (circles) and in an $In_{0.32}Ga_{0.68}As$ reference QW (squares) versus magnetic field, B. The continuous lines are fits of the variational method reported in Section 7.4.2 to the data. The exciton reduced mass resulting from the fit is reported.

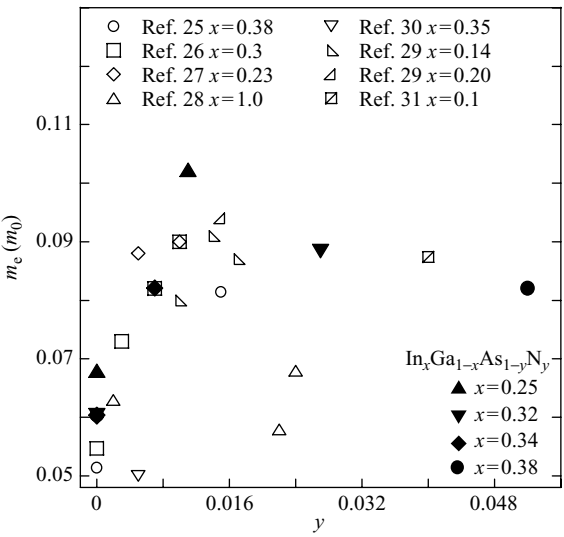

Figure 7.24. N concentration dependence of the electron effective mass m_e for the $In_xGa_{1-x}As_{1-y}N_y$ samples studied in this work (filled symbols) and taken from the literature (open symbols).

In $In_xGa_{1-x}As_{1-y}N_y$ the dependence of m_e (and r_{exc}, not shown here) on y shows two main differences with respect to the $GaAs_{1-y}N_y$ case. These quantities show a sizable change when $y \sim 1\%$ (one order of magnitude greater than the value found in $GaAs_{1-y}N_y$). In addition, the variation in m_e and r_{exc} occurs over a larger N concentration interval possibly due to different indium concentrations considered. These observations point toward a softening of N-related effects in $In_xGa_{1-x}As$, due to a lower degree of interaction between N states and the levels of continuum associated with the conduction band.

7.5. CONCLUSIONS

We studied the electronic properties of $In_xGa_{1-x}As_{1-y}N_y$/GaAs heterostructures by magneto-PL. The samples investigated cover a N compositional range spanning from the doping to the full alloy limit continuously. Several important aspects emerged from our investigations.

(i) We showed that magneto-PL as a function of temperature provides a new clue on the origin of radiative recombination at low temperatures in $In_xGa_{1-x}As_{1-y}N_y$. Indeed, the shift of the PL peak energy induced by B decreases sizably and changes its dependence on B from linear to quadratic when going from low to high temperatures. This counterintuitive result shows that the origin of the radiative recombination at low temperatures (T lower than 100 K) is not excitonic, contrary to the previous assignments, and is due to free holes recombining with electrons localized in N-rich regions.

(ii) The electron effective mass (and exciton wave function extent) is a much more insightful parameter than the bandgap energy in assessing the origin of the puzzling evolution of the electronic properties of dilute nitrides when the N concentration varies. Indeed, with increasing y the electron effective mass shows a sudden change for $y \sim 0.1\%$ (corresponding to a $GaAs_{1-y}N_y$ bandgap value of ~ 1.48 eV) within a very narrow interval of N concentrations. A crossing between the red shifting CBM extended states and one or more electronic levels in the gap due to N clusters is the likely physical origin of the sudden change in m_e (and r_{exc}). Qualitatively similar dependences of m_e and r_{exc} are found in $In_xGa_{1-x}As_{1-y}N_y$ alloys with $x \sim 30\%$. In this case a large variation in the electron effective mass and exciton radius occurs for $y \sim 1\%$.

(iii) Finally, our work indicates that an effective mass scheme is applicable also to $In_xGa_{1-x}As_{1-y}N_y$ notwithstanding the large fluctuations in the host crystalline potential, which are induced by N.

ACKNOWLEDGEMENTS

The authors thank A. Frova for his support throughout this work. We acknowledge the most fruitful collaboration with P.J. Klar and W. Stolz at Philipps-University, Marburg, Germany, and I.A. Buyanova and W.M. Chen at Linköping University, Sweden. We thank M. Stavola and F. Jiang at Leigh University, USA, for far-infrared measurements and fruitful discussions. We are grateful to A. Amore Bonapasta and F. Filippone (CNR-ISM, Roma, Italy) and V. Fiorentini and S. Sanna (Universita' di Cagliari, Italy) for sharing their theoretical calculations. We thank G. Ciatto (ESRF, Grenoble) and F. Boscherini (Universita' di Bologna, Italy) for X-ray diffraction measurements. We thank A. Vinattieri (Universita' of Firenze) and M. Geddo (Universita' of Parma, Italy) for valuable collaboration. We are grateful to A. Forchel (Wuerzburg, Universtity, Germany) for providing some of the samples studied. We thank A. Zunger and Y. Zhang at NREL, CO, USA for exchanging ideas. We are grateful to A. Miriametro and L. Ruggeri for very valuable technical assistance.

This work has been funded by Progetto Giovani Ricercatori, COFIN 2001 (MIUR), and FIRB (MIUR).

REFERENCES

[1] Weyers, M., Sato, M. & Ando, H. (1992) *Jpn. J. Appl. Phys.*, **31**, L853.
[2] Kondow, M., Uomi, K., Niwa, A., Kitatani, T., Watahiki, S. & Yazawa, Y. (1996) *Jpn. J. Appl. Phys.*, **35**, 1273.
[3] Xin, H.P. & Tu, C.W. (1998) *Appl. Phys. Lett.*, **72**, 2442.
[4] Perkins, J.D., Mascarenhas, A., Zhang, Y., Geisz, J.F., Friedman, D.J., Olson, J.M. & Kurtz, S.R. (1999) *Phys. Rev. Lett.*, **82**, 3312.
[5] Perlin, P., Subramanya, S., Mars, D.E., Kruger, J., Shapiro, N.A., Siegle, H. & Weber, E.R. (1998) *Appl. Phys. Lett.*, **73**, 3703.
[6] Shan, W., Walukiewicz, W., Ager, J.W., III, Haller, E.E., Geisz, J.F., Friedman, D.J., Olson, J.M. & Kurtz, S.R. (1999) *Phys. Rev. Lett.*, **82**, 1221.
[7] Klar, P.J., Grüning, H., Heimbrodt, W., Koch, J., Höhnsdorf, F., Stolz, W., Vicente, P.M.A. & Camassel, J. (2000) *Appl. Phys. Lett.*, **76**, 3439.
[8] Tsang, M.S., Wang, J.N., Ge, W.K., Li, G.H., Fang, Z.L., Chen, Y., Han, H.X., Li, L.H. & Pan, Z. (2001) *Appl. Phys. Lett.*, **78**, 3595.
[9] Fan, J.C., Hung, W.K., Chen, Y.F., Wang, J.S. & Lin, H.H. (2000) *Phys. Rev. B*, **62**, 10990.
[10] Grenouillet, L., Bru-Chevallier, C., Guillot, G., Gilet, P., Duvaut, P., Vannuffel, C., Million, A. & Chevanes-Paule, A. (2000) *Appl. Phys. Lett.*, **76**, 2241.
[11] Polimeni, A., Capizzi, M., Geddo, M., Fischer, M., Reinhardt, M. & Forchel, A. (2000) *Appl. Phys. Lett.*, **77**, 2870.
[12] Polimeni, A., Capizzi, M., Geddo, M., Fischer, M., Reinhardt, M. & Forchel, A. (2001) *Phys. Rev. B*, **63**, 195320.
[13] Suemune, I., Uesugi, K. & Walukiewicz, W. (2000) *Appl. Phys. Lett.*, **77**, 3021.
[14] Pinault, M.-A. & Tournié, E. (2001) *Appl. Phys. Lett.*, **78**, 1562.

[15] Kaschener, A., Lüttgert, T., Born, H., Hoffmann, A., Egorov, A.Yu. & Riechert, H. (2001) *Appl. Phys. Lett.*, **78**, 1391.

[16] Shirakata, S., Kondow, M. & Kitatani, T. (2001) *Appl. Phys. Lett.*, **79**, 54.

[17] Luo, X.D., Xu, Z.Y., Ge, W.K., Pan, Z., Li, L.H. & Lin, Y.W. (2001) *Appl. Phys. Lett.*, **79**, 958.

[18] Potter, R.J., Balkan, N., Carrère, H., Arnoult, A., Bedel, E. & Marie, X. (2003) *Appl. Phys. Lett.*, **82**, 3400.

[19] Zhang, Y., Mascharenas, A., Xin, H.P. & Tu, C.W. (2000) *Phys. Rev. B*, **61**, 7479.

[20] Hai, P.N., Chen, W.M., Buyanova, I.A., Xin, H.P. & Tu, C.W. (2000) *Appl. Phys. Lett.*, **77**, 1843.

[21] Wu, J., Shan, W., Walukiewicz, W., Yu, K.M., Ager, J.W., III, Haller, E.E., Xin, H.P. & Tu, C.W. (2001) *Phys. Rev. B*, **64**, 85320.

[22] Young, D.L., Geisz, J.F. & Coutts, T.J. (2003) *Appl. Phys. Lett.*, **82**, 1236.

[23] Wang, Y.J., Wei, X., Zhang, Y., Mascarenhas, A., Xin, H.P., Hong, Y.G. & Tu, C.W. (2003) *Appl. Phys. Lett.*, **82**, 4453.

[24] Jones, E.D., Allerman, A.A., Kurtz, S.R., Modine, N.A., Bajaj, K.K., Tozer, S.W. & Wie, X. (2000) *Phys. Rev. B*, **62**, 7144.

[25] Hetterich, M., Dawson, M.D., Egorov, A.Yu., Bernklau, D. & Riechert, H. (2000) *Appl. Phys. Lett.*, **76**, 1030.

[26] Pan, Z., Li, L.H., Lin, Y.W., Sun, B.Q., Jiang, D.S. & Ge, W.K. (2001) *Appl. Phys. Lett.*, **78**, 2217.

[27] Duboz, J.-Y., Gupta, J.A., Byloss, M., Aers, G.C., Liu, H.C. & Wasilewski, Z.R. (2002) *Appl. Phys. Lett.*, **81**, 1836.

[28] Hung, W.K., Cho, K.S., Chern, M.Y., Chen, Y.F., Shih, D.K., Lin, H.H., Lu, C.C. & Yang, T.R. (2002) *Appl. Phys. Lett.*, **80**, 796.

[29] Héroux, J.B., Yang, X. & Wang, W.I. (2002) *J. Appl. Phys.*, **92**, 4361.

[30] Ikari, T., Imai, K., Ito, A. & Kondow, M. (2003) *Appl. Phys. Lett.*, **82**, 3302.

[31] Gass, M.H., Papworth, A.J., Joyce, T.B., Bullough, T.J. & Chalker, P.R. (2004) *Appl. Phys. Lett.*, **84**, 1453.

[32] Geddo, M., Guizzetti, G., Capizzi, M., Polimeni, A., Gollub, D. & Forchel, A. (2003) *Appl. Phys. Lett.*, **83**, 470.

[33] Buyanova, I.A., Izadifard, M., Chen, W.M., Polimeni, A., Capizzi, M., Xin, H.P. & Tu, C.W. (2003) *Appl. Phys. Lett.*, **82**, 3662.

[34] Buyanova, I.A., Chen, W.M., Bergman, J.P., Monemar, B., Xin, H.P. & Tu, C.W. (1999) *Appl. Phys. Lett.*, **75**, 501.

[35] Mair, R.A., Lin, J.Y., Jiang, H.X., Jones, E.D. & Kurtz, S.R. (2000) *Appl. Phys. Lett.*, **76**, 188.

[36] Sun, H.D., Hetterich, M., Dawson, D.M., Egorov, A.Yu., Bernklau, D. & Riechert, H. (2002) *J. Appl. Phys.*, **92**, 1380.

[37] Vinattieri, A., Alderighi, D., Zamfirescu, M., Colocci, M., Polimeni, A., Capizzi, M., Gollub, D., Fischer, M. & Forchel, A. (2003) *Appl. Phys. Lett.*, **82**, 2805.

[38] Kurtz, S.R., Allerman, A.A., Seager, C.H., Sieg, R.M. & Jones, E.D. (2000) *Appl. Phys. Lett.*, **77**, 400.

[39] Teubert, J., Klar, P.J., Heimbrodt, W., Volz, K., Stolz, W., Thomas, P., Leibiger, G. & Gottschalch, V. (2004) *Appl. Phys. Lett.*, **84**, 747.

[40] Polimeni, A., Baldassarri HVH, G., Bissiri, M., Capizzi, M., Fischer, M., Reinhardt, M. & Forchel, A. (2001) *Phys. Rev. B*, **63**, 201304(R).

[41] Baldassarri HVH, G., Bissiri, M., Polimeni, A., Capizzi, M., Fischer, M., Reinhardt, M. & Forchel, A. (2001) *Appl. Phys. Lett.*, **78**, 3472.

[42] Polimeni, A., Bissiri, M., Augieri, A., Baldassarri, G., Capizzi, M., Gollub, D., Fischer, M., Reinhardt, M. & Forchel, A. (2002) *Phys. Rev. B*, **65**, 235325.

[43] Bissiri, M., Baldassarri, G., Polimeni, A., Gaspari, V., Ranalli, F., Capizzi, M., Amore Bonapasta, A., Jiang, F., Stavola, M., Gollub, D., Fischer, M. & Forchel, A. (2002) *Phys. Rev. B*, **65**, 235210.

[44] Polimeni, A., Baldassarri, G., Bissiri, M., Capizzi, M., Frova, A., Fischer, M., Reinhardt, M. & Forchel, A. (2002) *Semicond. Sci. Technol.*, **17**, 797.

[45] Bissiri, M., Baldassarri, G., Polimeni, A., Capizzi, M., Gollub, D., Fischer, M., Reinhardt, M. & Forchel, A. (2002) *Phys. Rev. B*, **66**, 033311.

[46] Klar, P.J., Gruning, H., Gungerich, M., Heimbrodt, W., Koch, J., Torunski, T., Stolz, W., Polimeni, A. & Capizzi, M. (2003) *Phys. Rev. B*, **67**, 121206(R).

[47] Polimeni, A., Bissiri, M., Felici, M., Capizzi, M., Buyanova, I.A., Chen, W.M., Xin, H.P. & Tu, C.W. (2003) *Phys. Rev. B*, **67**, 201303(R).

[48] Polimeni, A., Ciatto, G., Ortega, L., Jiang, F., Boscherini, F., Filippone, F., Amore Bonapasta, A., Stavola, M. & Capizzi, M. (2003) *Phys. Rev. B*, **68**, 085204.

[49] Polimeni, A., Baldassarri Höger von Högersthal, G., Masia, F., Frova, A., Capizzi, M., Sanna, S., Fiorentini, V., Klar, P.J. & Stolz, W. (2004) *Phys. Rev. B*, **69**, 041201(R).

[50] Kim, Y.-S. & Chang, K.J. (2002) *Phys. Rev. B*, **66**, 073313.

[51] Janotti, A., Zhang, S.B., Wei, S.-H. & Van de Walle, C.G. (2002) *Phys. Rev. Lett.*, **89**, 086403.

[52] Amore Bonapasta, A., Filippone, F., Giannozzi, P., Capizzi, M. & Polimeni, A. (2002) *Phys. Rev. Lett.*, **89**, 216401.

[53] Orellana, W. & Ferraz, A.C. (2002) *Appl. Phys. Lett.*, **81**, 3816.

[54] Janotti, A., Wei, S.-H, Zhang, S.B., Kurtz, S. & Van de Walle, C.G. (2003) *Phys. Rev. B*, **67**, 161201.

[55] Amore Bonapasta, A., Filippone, F. & Giannozzi, P. (2003) *Phys. Rev. B*, **68**, 115202.

[56] Amore Bonapasta, A., Filippone, F. & Giannozzi, P. (2004) *Phys. Rev. B*, **69**, 115207.

[57] Sanna, S. & Fiorentini, V. (2004) *Phys. Rev. B*, **69**, 125208.

[58] Jiang, F., Stavola, M., Capizzi, M., Polimeni, A., Amore Bonapasta, A. & Filippone, F. (2004) *Phys. Rev. B*, **69**, 041309(R).

[59] Oueslati, M., Benoit a la Guillaume, C. & Zouaghi, M. (1988) *Phys. Rev. B*, **37**, 3037.

[60] Ouadjaout, D. & Marfaing, Y. (1990) *Phys. Rev. B*, **41**, 12096.

[61] Aït-Ouali, A., Yip, R.Y.-F., Brebner, J.L. & Masut, R.A. (1998) *J. Appl. Phys.*, **83**, 3153.

[62] Kim, H.S., Mair, R.A., Li, J., Lin, J.Y. & Jiang, H.X. (2000) *Appl. Phys. Lett.*, **76**, 1252.

[63] Cohen, E. & Sturge, M.D. (1982) *Phys. Rev. B*, **25**, 3828.

[64] Ouadjaout, D. & Marfaing, Y. (1992) *Phys. Rev. B*, **46**, 7908.

[65] Aït-Ouali, A., Chennouf, A., Yip, R.Y.-F., Brebner, J.L., Leonelli, R. & Masut, R.A. (1998) *J. Appl. Phys.*, **84**, 5639.

[66] Buyanova, I.A., Chen, W.M., Pozina, G., Bergman, J.P., Monemar, B., Xin, H.P. & Tu, C.W. (1999) *Appl. Phys. Lett.*, **75**, 501.

[67] Yang, H.C., Kuo, P.F., Lin, T.Y., Chen, Y.F., Chen, K.H., Chen, L.C. & Chyi, J.I. (2000) *Appl. Phys. Lett.*, **76**, 3712.

[68] Halperin, B. & Lax, M. (1996) *Phys. Rev.*, **148**, 722.

[69] Cohen, E. & Sturge, M.D. (1982) *Phys. Rev. B*, **25**, 3828.

[70] Sun, B.Q., Gal, M., Gao, Q., Tan, H.H. & Jagadish, C. (2002) *Appl. Phys. Lett.*, **81**, 4368.

[71] Bayer, M., Walck, S.N., Reinecke, T.L. & Forchel, A. (1998) *Phys. Rev. B*, **57**, 6584.

[72] Baldassarri Hoeger von Hoegersthal, G., Polimeni, A., Masia, F., Bissiri, M., Capizzi, M., Gollub, D., Fischer, M. & Forchel, A. (2003) *Phys. Rev. B*, **67**, 233304.

[73] Hopfield, J.J., Thomas, D.G. & Lynch, R.T. (1966) *Phys. Rev. Lett.*, **17**, 312.

[74] Rossi, J.A., Wolfe, C.M. & Dimmock, J.O. (1970) *Phys. Rev. Lett.*, **25**, 1614.
[75] Rühle, W. & Göbel, E. (1976) *Phys. Stat. Sol. (b)*, **78**, 311.
[76] Bimberg, D. (1978) *Phys. Rev. B*, **18**, 1794.
[77] Dean, P.J., Venghaus, H. & Simmonds, P.E. (1978) *Phys. Rev. B*, **18**, 6813.
[78] Zemon, S., Norris, P., Koteles, E.S. & Lambert, G. (1986) *J. Appl. Phys.*, **59**, 2828.
[79] Zheng, X.L., Heiman, D., Lax, B., Chambers, F.A. & Stair, K.A. (1988) *Appl. Phys. Lett.*, **52**, 98.
[80] Skromme, B.J., Bhat, R., Koza, M.A., Schwarz, S.A., Ravi, T.S. & Hwang, D.M. (1990) *Phys. Rev. Lett.*, **65**, 2050.
[81] Masia, F., Polimeni, A., BaldassarriHöger von Högersthal, G., Bissiri, M., Capizzi, M., Klar, P.J. & Stolz, W. (2003) *Appl. Phys. Lett.*, **82**, 4474.
[82] Polimeni, A., Masia, F., Vinattieri, A., Baldassarri Höger von Högersthal, G. & Capizzi, M. (2004) *Appl. Phys. Lett.*, **84**, 2295.
[83] Vurgaftman, I., Meyer, J.R. & Ram-Mohan, L.R. (2001) *J. Appl. Phys.*, **89**, 5815.
[84] Kent, P.R.C. & Zunger, A. (2001) *Phys. Rev. B*, **64**, 115208.
[85] (a) Shtinkov, N., Desjardins, P. & Masut, R.A. (2003) *Phys. Rev. B*, **67**, 081202(R); (b) Lindsay, A., Tomic, S. & O'Reilly, E.P. (2003) *Solid State Electron.*, **47**, 443 and references therein.
[86] Grüning, H., Chen, L., Hartmann, T., Klar, P.J., Heimbrodt, W., Höhnsdorf, F., Koch, J. & Stolz, W. (1999) *Phys. Stat. Sol. (b)*, **215**, 39.
[87] Makimoto, T. & Kobayashi, N. (1995) *Appl. Phys. Lett.*, **67**, 688.
[88] Shima, T., Makita, Y., Kimura, S., Sanpei, H., Fukuzawa, Y., Sandhu, A. & Nakamura, Y. (1999) *Appl. Phys. Lett.*, **74**, 2675.
[89] Makimoto, T., Saito, H., Nishida, T. & Kobayashi, N. (1997) *Appl. Phys. Lett.*, **70**, 2984.
[90] Zhang, Y., Mascarenhas, A., Geisz, J.F., Xin, H.P. & Tu, C.W. (2001) *Phys. Rev. B*, **63**, 085205.
[91] Francoeur, S., Nikishin, S.A., Jin, C., Qiu, Y. & Temkin, H. (1999) *Appl. Phys. Lett.*, **75**, 1538.
[92] Tisch, U., Finkman, E. & Salzman, J. (2002) *Appl. Phys. Lett.*, **81**, 463.
[93] Lindsay, A. & O'Reilly, E.P., private communication.
[94] Mattila, T., Wei, Su.-H. & Zunger, A. (1999) *Phys. Rev. B*, **60**, R11245.
[95] Walck, S.N. & Reinecke, T.L. (1998) *Phys. Rev. B*, **57**, 9088.
[96] Yang, S.-R. & Sham, L.J. (1987) *Phys. Rev. Lett.*, **58**, 2598.
[97] Bauer, G.E.W. & Ando, T. (1988) *Phys. Rev. B*, **37**, 3130(R).
[98] Zheng, X.L., Heiman, D. & Lax, B. (1989) *Phys. Rev. B*, **40**, 10523.
[99] Hou, H.Q., Staguhn, W., Takeyama, S., Miura, N., Segawa, Y., Aoyagi, Y. & Namba, S. (1991) *Phys. Rev. B*, **43**, 4152.
[100] Lee, K.-S., Aoyagi, Y. & Sugano, T. (1992) *Phys. Rev. B*, **46**, 10269.
[101] Lee, K.S. & Lee, E.-H. (1994) *J. Appl. Phys.*, **76**, 5778.
[102] Klar, P.J., Grüning, H., Koch, J., Schäfer, S., Volz, K., Stolz, W., Heimbrodt, W., Kamal Saadi, A.M., Lindsay, A. & O'Reilly, E.P. (2001) *Phys. Rev. B*, **64**, 121203(R).
[103] Kurtz, S., Webb, J., Gedvikas, L., Friedman, D., Geisz, J., Olson, J., King, R., Joslin, D. & Karam, N. (2001) *Appl. Phys. Lett.*, **78**, 748.
[104] Kim, K. & Zunger, A. (2001) *Phys. Rev. Lett.*, **86**, 2609.
[105] Ciatto, G., D'Acapito, F., Grenouillet, L., Mariette, H., De Salvador, D., Bisognin, G., Carboni, R., Floreano, L., Gotter, R., Mobilio, S. & Boscherini, F. (2003) *Phys. Rev. B*, **68**, 161201(R).
[106] Wimbauer, Th., Oettinger, K., Efros, Al.L., Meyer, B.K. & Brugger, H. (1994) *Phys. Rev. B*, **50**, 8889.